

# Strength and structural barrier function of steel channel-reinforced concrete composite slabs

Katsuhiko Emori†

*Department of Architecture, Maebashi Institute of Technology  
460-1, Kamisadori-machi, Maebashi-ci, Gunma Pref., 371-0816, Japan*

*(Received April 10, 2002, Accepted July 8, 2003)*

**Abstract.** This paper reports on the development of a new composite slab system that uses a large-lipped steel channel and reinforced concrete. The advantages of this new system are that it serves as both a structural unit and an unsupported form and it has a secondary structural barrier function. A concrete pouring test was carried out for the large-lipped steel channel. Full-scale tests were carried out to assess the flexural strength-deformation characteristics and structural mechanics of the composite slab. The barrier mechanics of the steel channel concrete element (referred to as the SC subunit) of the composite slab are examined. The test results indicate that the new composite slab has excellent strength, ductility characteristics, and a structural barrier function in its SC subunit that is highly effective against severe loading.

**Key words:** large-lipped steel channel; composite slab; flexural strength; structural barrier function; structural index.

---

## 1. Introduction

Metal decking is commonly used in construction sites worldwide as a temporary forming material to reduce work involving reinforced concrete slab structures. It also serves as a slab reinforcement substructure in resisting loads after the concrete hardens (ASCE (1991), Eurocode 4 (1994), and JSCE (1989)).

During the past ten years, new steel-concrete composite slab systems have been studied and proposed by many researchers and engineers. Patrick *et al.* (1995) reported limit-state design rules for composite slabs incorporating Bondeck II profiled steel sheeting in steel-frame buildings. McDonald *et al.* (1995) proposed a new steel and concrete domestic flooring system for housings, namely, Unifloor, a suspended floor system. AISC (1999) adopted the AISC Load and Resistance Factor Design Specification in 1986 for composite floor systems. Ma *et al.* (2001) proposed a new type of steel-concrete composite plate that covers long spans and large spaces. This SC roof/floor structure is a grid plane and a three-dimensional load-bearing plate. They report that the decrease of self-weight improves static and seismic mechanic characteristics and reduces construction time. Buckner (Subcommittee chairman on composite construction, ASCE, 2002) reported an overview of construction methods for composite steel-concrete floor systems in U. S. buildings, such as composite beams, dead load deflection limits, steel decks, shear stud installations, and concrete slab finishes.

This paper reports the development of a new composite slab system of the (RC+SC) integrated

---

†Professor

composite slab that uses a large-lipped steel channel (S) and reinforced concrete (RC). It also reports the results of structural tests conducted with this system. This new structural system is more effective than conventional decking-based techniques, serving as both a structural unit and an unsupported form. It thus reduces construction time and costs. It also has a secondary structural barrier function in the lower steel channel concrete element (hereafter referred to as the SC subunit) of the composite slab that is effective against severe loadings, (Emori 2001). Frangopol and Curley (1987) reported the effects of damage and redundancy on structural reliability and discussed the concept of “fail-safe” structures. Iyama and Kuwamura (1998) proposed the concept of “fail-safe” structures to resist massive earthquakes in studies of the barrier mechanics of structures. The word “fail” in this context indicates conditions when a structural subelement of the overall structural system collapses during massive earthquakes. The word “safe” implies that the overall structural system does not collapse during massive earthquakes. For example, a moment-resisting frame structure with braces is a “fail-safe” structure, which is defined as a system in which the subsystem (brace) collapses (section fracture) to prevent the collapse of the entire system (the frame structure).

Steel sheets such as Metal Deck have been studied by many researchers as platforms, concrete formworks, and as a standard structural subelement of composite steel-concrete floor (slab). However, it has not been studied with respect to structural barrier (fail-safe) functions in composite slab structures.

This paper first presents full scale tests for concrete pouring and flexural strength, and then, from the test results, this structural barrier (fail-safe) concept is studied and applied for the (RC+SC) integrated composite slab to be used in specific heavy structures.

The concept of the secondary structural barrier function of the lower SC subunit (a structural subelement) of this composite slab structure (the overall structural system) for extremely severe load, is proposed and explained in this study.

## 2. Proposed composite slab

The proposed six-meter-long, 50 cm thick composite slab system and its sections are shown in Figs. 1 and 2. A large-lipped steel channel of U-900×250×100×6 is positioned at the bottom of the composite slab. Its side web plates are connected by M16 high-tension bolts (@900) and the top part is reinforced

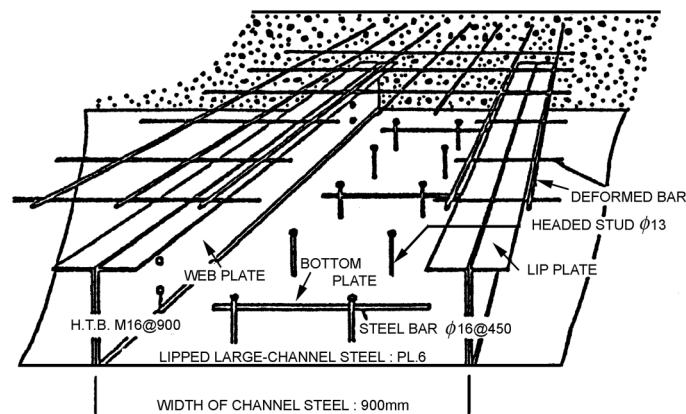


Fig. 1 New composite slab system

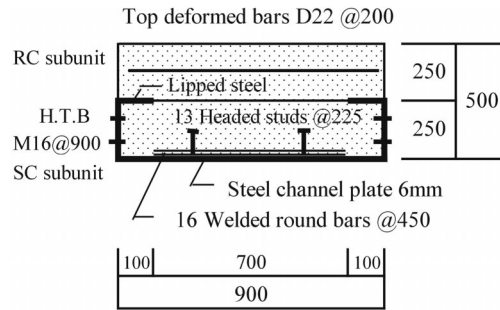


Fig. 2 One unit section of lipped steel channel and reinforced concrete composite slab

by D22 deformed bars (@200). Round bars ( $\Phi$  16, @450) are welded to the bottom plate of the steel channel to stiffen it and reduce flexural deformation when concrete is poured into it. Headed studs ( $\Phi$  13, @225) are used for the shear connection since they integrate the structural functions of both steel and concrete. The large-lipped steel channel works as a form when concrete is poured during construction. The slab structure, of which the steel channel is a part, acts as a composite load-bearing slab after the completion of the structure, since it also carries vertical service design loads. The steel plates of the composite slab work in this capacity as tension material to accommodate positive flexural stress, and the top deformed bars work as tension material to accommodate negative flexural stress. The composite slab consists of an upper RC subunit and a lower SC subunit, as shown in Fig. 2. The slab thickness of the composite slab is determined to preserve the required in-plane stiffness or to satisfy the function as a shield slab rather than its required strength. This composite slab has been developed for use as a standard floor slab (design load of 0.02 MN/m<sup>2</sup>) in projects such as marine environments and nuclear-related structures, (Emori 1999).

2.1. Structural barrier function

The proposed (RC+SC) integrated composite slab has a secondary structural barrier function, in that the lower SC subunit can resist very severe loading, such as that imposed by low frequency but heavy shock loads. The load-deflection characteristics obtained by flexural strength tests revealed that the lower SC subunit had high ductility and flexural strength even when the upper RC subunit failed completely. The basic concept of the secondary structural barrier function of the proposed composite slab is shown in Fig. 3. The (RC+SC) integrated composite slab supports design loads for both long-

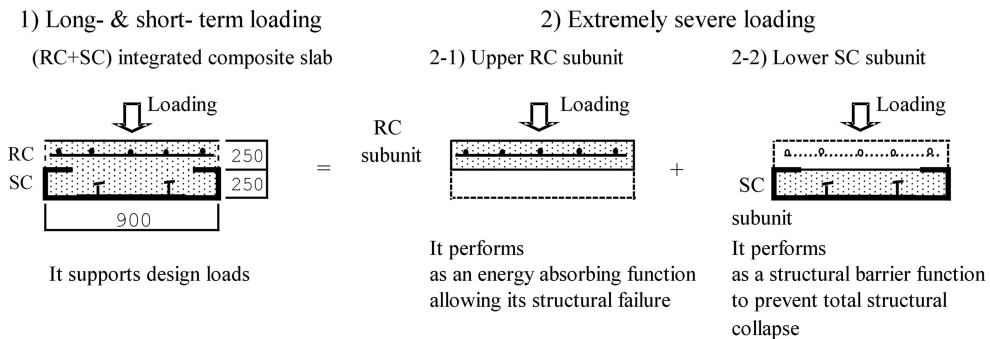


Fig. 3 Concept of secondary structural barrier function of (RC+SC) integrated composite slab

and short-term loading. In addition, an upper RC slab subunit performs as an energy-absorbing function that allows its structural failure in extremely severe loading situations that are beyond the design specifications. A lower SC slab subunit performs as a structural barrier function to prevent total structural collapse (due to flexural failure). The concept of the structural barrier function can be applicable to structures with redundancy in the load bearing capacity of the system. The barrier mechanics of the SC sub unit were examined based on the test results and are explained by an impact load example.

### 3. Test programs

Full-scale tests for concrete pouring and flexural strength were conducted to clarify the structural behavior and integrity of the proposed composite slab; they are depicted in Fig. 4, (Kato *et al.* 1988). The concrete mix proportions are shown in Table 1. The mechanical properties of the concrete and steel used in the tests are shown in Tables 2 and 3. Specimens No. 1 and No. 2 in Table 2 correspond to the proposed composite slabs with and without a concrete pouring load.

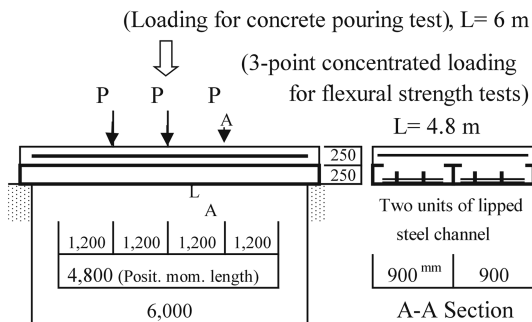


Fig. 4 Outlines of concrete pouring and flexural strength tests

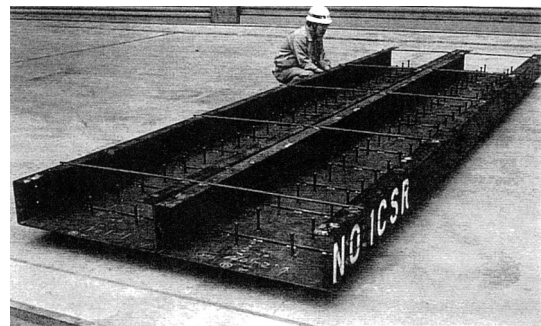


Fig. 5 Two units of large-lipped steel channel

Table 1 Concrete mix proportions

Fine aggregate ( $\text{kN/m}^3$ )	Coarse aggregate ( $\text{kN/m}^3$ )	Fine aggregate ratio (%)	Cement (C) ( $\text{kN/m}^3$ )	Water (W) ( $\text{kN/m}^3$ )	W/C (%)	Admixture ( $\text{kN/m}^3$ )	Slump (cm)
7.75	9.97	44.4	3.19	1.69	53	0.008	14.5

Table 2 Mechanical properties of concrete

Specimen (No.)	Compressive strength (MPa)	Tensile strength (MPa)	Elastic modulus ( $\times 10^3$ MPa)	Age (Days)
1	28.8	2.4	24.2	28
2	31.3	2.6	24.6	57

No.1: Concrete pouring test + Flexural strength test

No.2: Flexural strength test

Table 3 Mechanical properties of steel

Member	Type	Steel grade	Yield stress $\sigma_y$ (MPa)	Tensile strength $\sigma_u$ (MPa)	Elongation (%)
Steel channel	PL-6	SS400	273	426	23.0
Deformed bar	D22	SD345	383	603	21.4
Round bar	$\Phi$ 16	SR235	344	480	30.7
Headed stud	$\Phi$ 13×120	SS400	377	481	32.3

### 3.1. Concrete pouring tests

Concrete was poured into two lipped steel channel units with span lengths of 6 m to create a composite slab with a thickness of 50 cm, as shown in Fig. 4. Fig. 5 contains a photograph of two full-scale units of a large-lipped steel channel assembled on the floor. Test specimen No. 1 was used in the concrete pouring test to determine whether the steel channel is suitable as an unsupported form. The flexural deformations were measured, including the steel stresses and strains at the centers of the longitudinal and width spans of the bottom steel plates. These values were also computed using the elastic beam theory for the longitudinal span and by frame analysis modeling of a cross section of the steel channel as line elements with a unit width of 1 m.

### 3.2. Flexural strength tests

Full-scale flexural strength tests were performed to examine the load-deflection characteristics and flexural strength of the composite slab. The two test specimens shown in Table 2 were prepared with and without stress from the concrete pouring load and were tested to examine the load-deflection characteristics and flexural strength of the composite slab. One objective of this study was to assess the flexural deformation of and initial stress on the steel channel caused by the load of the concrete, and hence its impact on the composite slab strength. The other objective of this study was to examine the load-deflection characteristics and structural mechanics of the composite slab which represent the composite interactions among the (RC+SC) integrated composite slab, its upper and lower subunits, and the reinforced concrete (RC) and steel channel concrete (SC).

A three-point concentrated loading test was conducted in which the positive bending part of the steel plate (span  $L = 4.8$  m) yielding tension had approximately the same bending moment distribution as a uniform loading situation, as illustrated in Fig. 4. Fig. 6 shows the test set-up to perform the flexural strength tests. The test specimens were set in the stiff portal steel frame. The load was applied through three hydraulic jacks with 1.96 MN bearing capacity and was recorded by load cells using digital recording. The loading was performed by gradually increasing/decreasing the amplitude through seven cycles until the deflection rate (central deflection/span:  $\delta/L$ ) became 1/30 as shown in Fig. 7. We measured the flexural deflection of the test specimen and the stresses and strains of the steel plates. Fig. 8 shows the measurements and instrumentation system for the flexural strength tests. Computation models to obtain the load-deflection relationship of the composite slab were shown for the three points where flexural cracking, channel bottom steel plate yielding, and top concrete crushing exhibited the ultimate strength (see Table 4). The following conditions were assumed in the calculations using the conventional beam theory. 1) The cross section of the composite slab remains planar under the load, and only bending deformation is considered. 2) The stress-strain relationship for the steel plate is purely

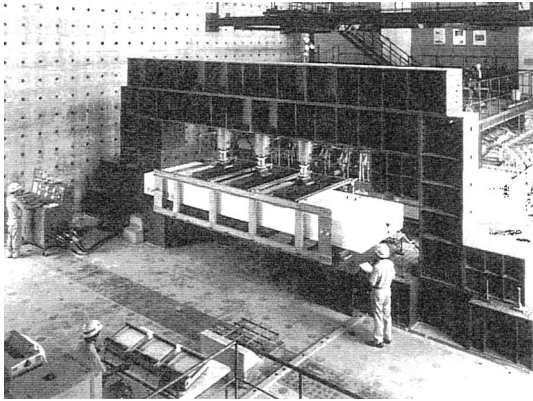


Fig. 6 Test set-up for flexural strength tests

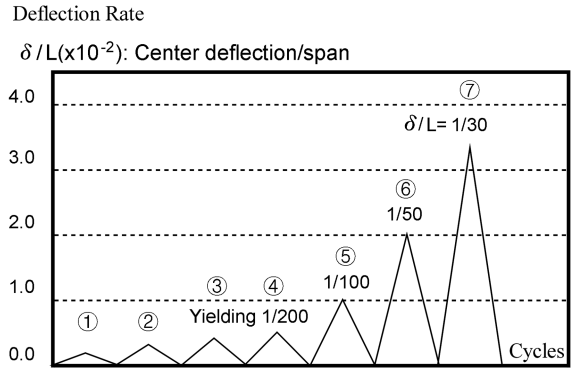
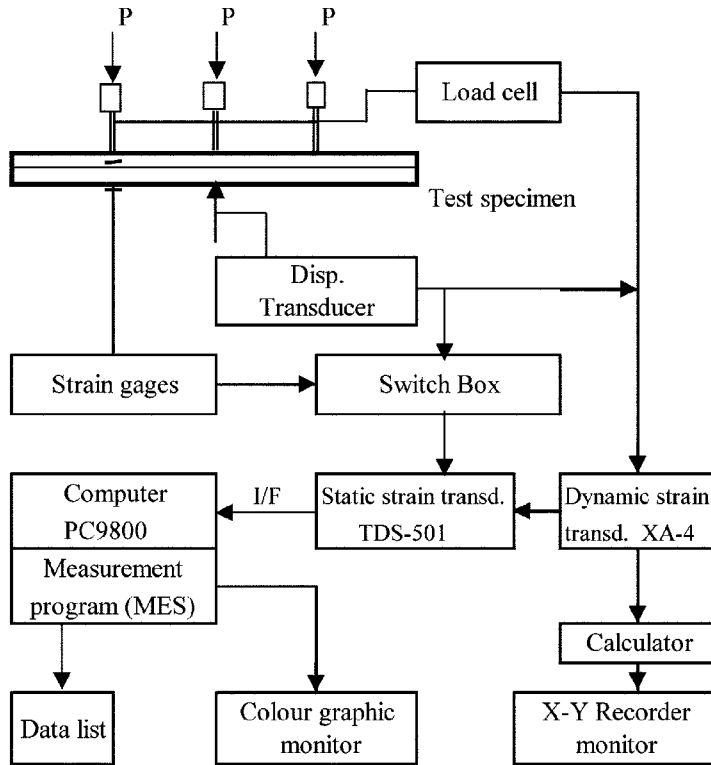


Fig. 7 Loading cycles for flexural strength tests



- Measurement items
- 1) Vertical loads
  - 2) Vertical disp. and slippage between S and C
  - 3) Strains of steel and rebars

Fig. 8 Measurements and instrumentation system for flexural strength tests

elasto-plastic, and 3) An e-function assumption method is applied for the concrete compressive stress-strain relationship (Muto 1964).

Table 4 Computation models for load-deflection relationship of (RC+SC) integrated composite slab

Distribution	At flexural cracking	At yielding of bottom plate	At crushing of top concrete
Strain	<p>Compression 250 mm 250 mm Tension <math>\epsilon_{ct}</math></p>	<p><math>\epsilon_{sy}</math></p>	<p><math>\epsilon = 3000\mu</math></p>
Stress	<p>C: Concrete Rebar R Sl Sw Sb</p>	<p>C R Sl Sw Sb</p>	<p>C R Sl Sw Sb</p>

$\epsilon_{ct} = 1.5 \cdot f_{ct} / E_c$        $f_{ct}$ : Tensile strength of concrete  
 $\epsilon_{sy} = \sigma_y / E_s$        $\epsilon_y$ : Yield stress of steel  
 $E_c, E_s$ : Young's moduli of concrete and steel  
 Sl, Sw, Sb: Tension forces at lipped, web, bottom plate of steel channel

#### 4. Test results

##### 4.1. Concrete pouring test results

Results of the concrete pouring tests and the computed deflection values for the lipped steel channel are shown in Table 5. The maximum flexural deformations at the centers of the longitudinal and width spans of the bottom steel plates were 10.28 mm and 3.13 mm, as shown in Table 5 and Fig. 9. These deformations approximately satisfied the design target values for form members (AIJ standard, 1998) of 20 mm (= span/300) and 3.0 mm (= width/300). Deflection in the width span was reduced by the stiffening effect of the bottom steel plate by welding  $\Phi$  16 round bars (@450). The stresses in the longitudinal direction of the lipped plate and in the longitudinal and width directions of the bottom plate of the steel channel were -102.7 Mpa (compression), 42.4 MPa and 64.7 MPa, as shown in Table 5. These stresses of the steel plates were all below the long-term allowable stress of 157 MPa. The proposed composite slab using a large-lipped steel channel can serve as an unsupported form in slab construction.

Table 5 Concrete pouring test and computed results for lipped steel channel

Specimen (No.)	Test values at center of span					Computed values at center of span			
	Max. defl. (mm)		Stress (MPa)			Max. deflection (mm)			
	In longi. direction	In width direction	Lip part of channel	Bottom plate of channel		In longitudinal direction		In width direction	
	$\delta_{el}$	$\delta_{es}$	In longi. direction (comp.)	In longi. direction $\sigma_{yc}$	In width direction $\sigma_{xc}$	$\delta_{cl}$	(Ratio) $\delta_{el} / \delta_{cl}$	$\delta_{cs}$	(Ratio) $\delta_{es} / \delta_{cs}$
1	10.28	3.13	-102.7	42.4	64.7	10.06	1.02	3.17	0.99

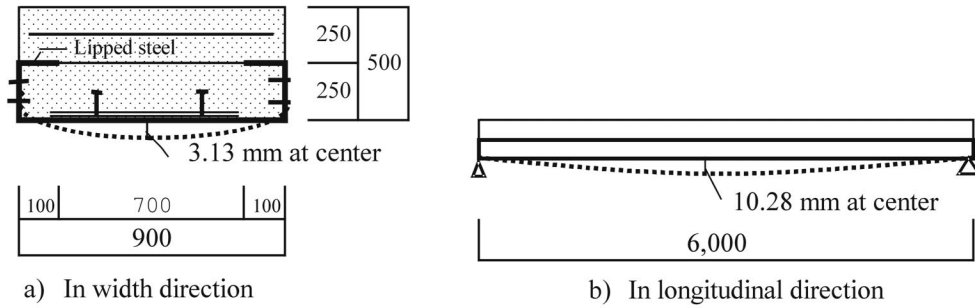


Fig. 9 Bottom plate deflection of lipped steel channel in concrete pouring test

4.2. Flexural strength test results

The structural behavior of test specimen No. 1 during the flexural strength test is shown in Table 6. The results of the flexural strength tests for test specimens No. 1, 2 and the computed values are given in Table 7. The load-deflection envelope curves for test specimens No. 1 and No. 2 are shown in Fig. 10. The uniform long-term design load of 0.02 MN/m<sup>2</sup> corresponds to the  $P = 0.042$  MN three-point loading of the specimen. The bond between the lip part of the steel plate and the concrete failed at load  $P = 0.245$  MN for test specimen No. 1 at about a quarter-span from the support, leading to a small reduction in rigidity. Flexural shear cracking occurred at the center of the span at load  $P = 0.445$  MN. The steel channel bottom plate yielded at around  $P = 0.5$  MN, but the strength increased. Shear cracking

Table 6 Structural behavior of test specimen No. 1 during flexural strength test

Loading		Defl.	Test specimen Two units of the (RC+SC) composite slab
Cyc.	$P$ (MN)	$\delta$ (mm)	
1	0.042	0.4	At design load level of 0.02 MN/m <sup>2</sup>
2	0.085	0.8	At twice design load level
3	0.245	3.2	① Bond failure between concrete and lip part of steel channel
	0.445	8.1	② Flexural shear cracking
4	0.493	9.3	③ Tension yielding at bottom plate of the steel channel
	0.747	23.8	$\delta / L$ (central deflection/span length) $\doteq$ (1/200)
5	0.779	28.3	④ Shear cracking
	0.809	37.7	⑤ Concrete crushing, at ultimate strength
6	0.771	47.8	$\delta / L \doteq$ (1/100)
	0.735	49.5	Compression failure of upper rebars
7	0.630	84.7	$\delta / L \doteq$ (1/50)
	0.541	105.1	Partial compression yielding of lip part of the steel channel and compression buckling of top rebars
	0.514	159.7	$\delta / L \doteq$ (1/30): Partial buckling of lip part of the steel channel.

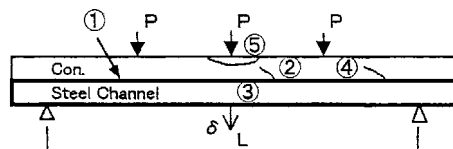


Table 7 Flexural strength test and computed results for (RC+SC) integrated composite slabs

Specimen	Test values						Computed values					
	Load at bond failure between concrete & lipped steel	Load at flexural shear cracking	Load at bottom plate yielding	Load at ultimate strength	Elastic rigidity	Stress* of bottom plate at design load (0.042 MN)	Load at bottom plate yielding	Load at ultimate strength	Elastic rigidity			
(NO.)	(MN)	(MN)	$P_{ey}$ (MN)	$P_{em}$ (MN)	$K_e$ (MN/mm)	$\sigma_{yb}$ (MPa)	$P_{cy}$ (MN)	(Ratio) $\frac{P_{ey}}{P_{cy}}$	$P_{cm}$ (MN)	(Ratio) $\frac{P_{em}}{P_{cm}}$	$K_c$ (MN/mm)	(Ratio) $\frac{K_e}{K_c}$
1	0.245	0.445	0.493	0.809	0.123	6.8	0.574	0.86	0.794	1.02	0.113	1.09
2	0.148	0.148	0.470	0.808	0.119	-	0.655	0.72	0.813	0.99	0.113	1.04

\*: Stress in the longitudinal direction of bottom steel plate at center of the span

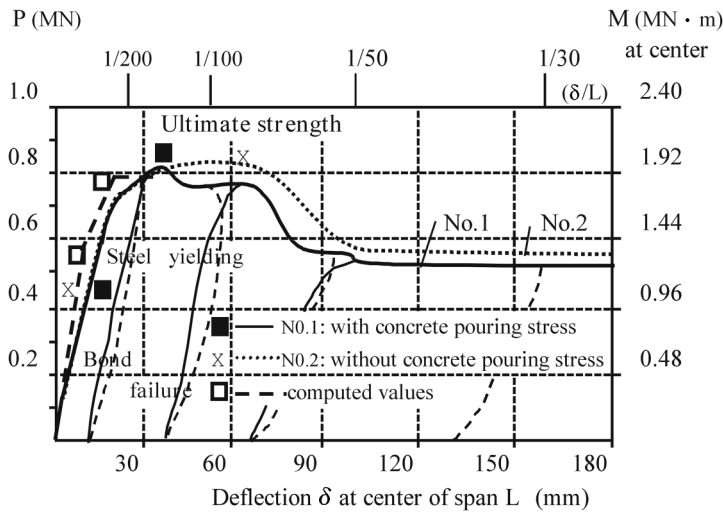


Fig. 10 Load-deflection envelope curves for test specimens No. 1 and No. 2 under flexural strength tests

occurred at load  $P = 0.779$  MN near the support. The concrete crushed at around  $P = 0.8$  MN, leading to the ultimate strength. Both the strength and stiffness subsequently decreased. The lip part of the steel channel partially yielded under compression and the top compression bars also buckled at load  $P = 0.541$  MN. Finally, the lip part of the steel channel buckled locally at load  $P = 0.514$  MN, at about  $\delta/L=1/30$ . No stress effect on the steel channel plate caused by the pouring of the concrete was observed on the load-deflection envelope curve of the composite slab, but there was a difference after the slab’s ultimate strength was reached, as shown in Fig. 10.

Fig. 11 shows the slippage along the span length between the lip part of the steel channel and the concrete under the flexural strength tests. The slippage at the ultimate strength was minimal, less than 1 mm, and became the maximum value of about 2 mm at the level of  $\delta/L=1/30$ . The integrated composite slab exhibited the ultimate strength by integrating the structural functions of both steel and concrete.

Fig. 12 shows the strain distribution across the cross section at the center of the span of the test specimen No. 1. The strains at the lip part and bottom plate of the steel channel when concrete poured were  $-499 \times 10^{-6}$ ,  $206 \times 10^{-6}$ . The strain distribution across the cross section of the composite slab at the ultimate strength indicates that the small parts of the upper RC subunit, including the compression top

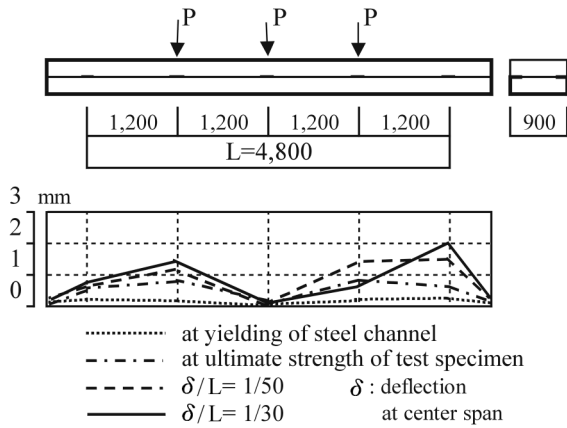


Fig. 11 Slippage between lip part of steel and concrete of test specimen No. 1 under flexural strength test

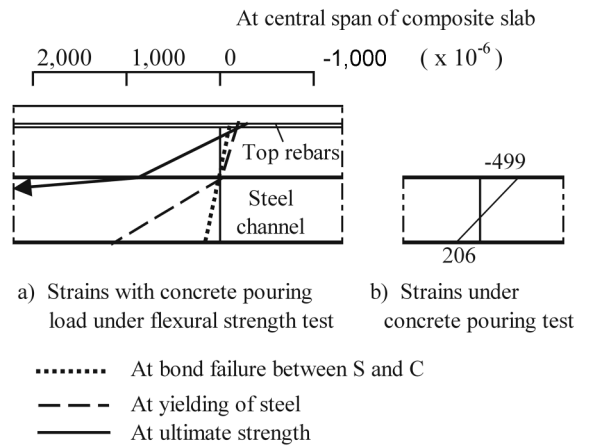
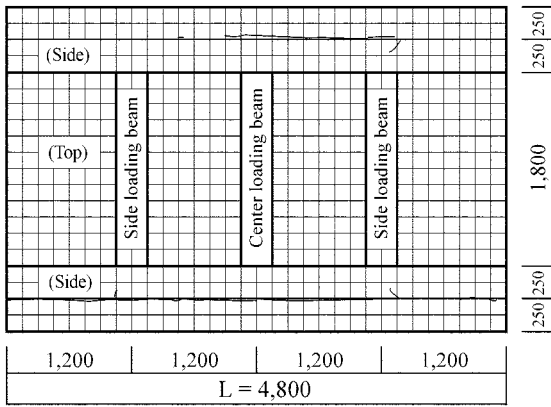
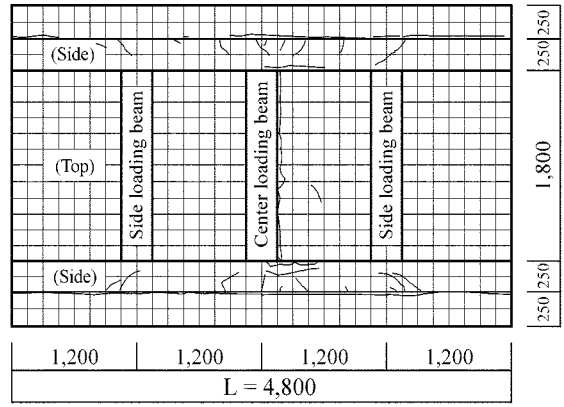


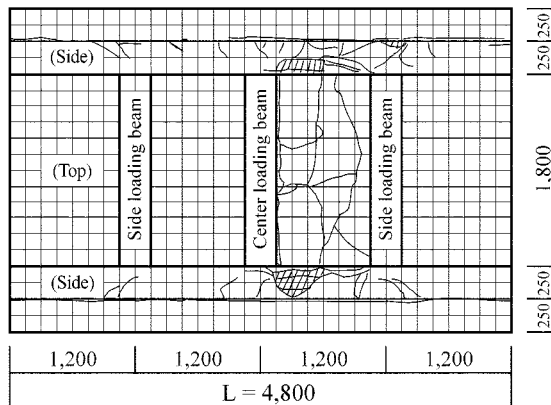
Fig. 12 Strain distributions across the cross section of test specimen No. 1



(a) At yielding of channel bottom plate



(b) At  $\delta/L = 1/100$



(c) At  $\delta/L = 1/30$   $\delta$ : center deflection

Fig. 13 Crack patterns of test specimen No. 1 under flexural strength test

reinforcing bars, resist compression stress (strain) of the cross section of the composite slab. In contrast, the lower SC subunit resists the overall tension stress (strain) of the cross section of the composite slab. Fig. 13 shows the crack patterns of the test specimen at three stages during the test, i.e., at the yielding of the steel channel bottom plate, at the deflection of the center span / span length ( $\delta/L$ )=1/100, and at  $\delta/L = 1/30$ .

A photograph of the test specimen No. 1 after failure is shown in Fig. 14. The test specimen failed due to crushing of the concrete of the upper RC subunit at the center of the span of the composite slab. However, the lower SC subunit still did not fail and preserve the load-bearing capacity, as the photograph indicates. Shear connectors of headed studs, welded to the bottom of the steel plate, integrated the structural functions of both steel and concrete and hence contributed to preserve the load-bearing capacity of the lower SC subunit.

The computed load-deflection curve up to the ultimate strength is also shown by the thick broken line in Fig. 10. The computation results shown in Table 7 indicate that the elastic rigidity and ultimate strength roughly agree with the test results. However, the computed values for the flexural yielding loads were greater than the test values. The increase in strength after the yielding of the steel channel bottom plate in the test can also be seen in the computation curve shown in Fig. 10. This increase results from the lip and web of the channel steel part bearing the tension stress of the cross section. The integrated composite slab in this system has considerable redundancy in its load bearing capacity.

The combined tensile stress  $\sigma$  of the bottom steel plate of the steel channel is computed by Eq. (1) for a long-term design load.

$$\sigma = \sqrt{\sigma_{xc}^2 + (\sigma_{yc} + \sigma_{yb})^2} \quad (1)$$

Here,  $\sigma_{xc}$  and  $\sigma_{yc}$  are the tensile stresses at the center span in the width and longitudinal directions of the bottom plate of the steel channel due to the concrete pouring load.  $\sigma_{yb}$  (= 6.8 MPa in Table 7) is the tensile stress at the center span in the longitudinal direction of the bottom plate of the steel channel due to three point loading  $P=0.042$  MN after the concrete hardens. The combined tensile stress  $\sigma=81.3$  MPa can be obtained by substituting the corresponding values of  $\sigma_{xc}=64.7$  MPa,  $\sigma_{yc}=42.4$  MPa, and  $\sigma_{yb}$  shown in Tables 5 and 7 into Eq. (1). The computed combined tensile stress  $\sigma$  of the bottom plate was below the long-term allowable tensile stress of 157 MPa. The composite slab has sufficient redundancy in the flexural strength of the system for a long-term design load.

## 5. Secondary structural barrier function of the (RC+SC) composite slab

The load-deflection envelope curves depicted in Fig. 10, the structural behavior in the test shown in Table 6, and the test specimen after failure shown in Figs. 14 (a) and (b) all indicate that the (RC+SC) integrated composite slab has sufficient strength and ductility. Part of the upper reinforced concrete (RC) subunit started crushing at a center deflection of 30 to 40 mm, but the overall composite slab maintained its strength to a center deflection of 60 to 70 mm. Part of the upper RC subunit then broke off, and its strength was reduced to about 60% of the strength of the overall composite slab. The composite slab subsequently maintained its flexural strength to a deflection of more than 160 mm (central deflection/span length:  $\delta/L = 1/30$ ) at the central span.

The ultimate flexural strength of both the (RC+SC) integrated composite slab and the lower SC subunit were computed assuming a block compressive stress of  $0.85F_c$  for concrete and a tensile strength of  $\sigma_u$

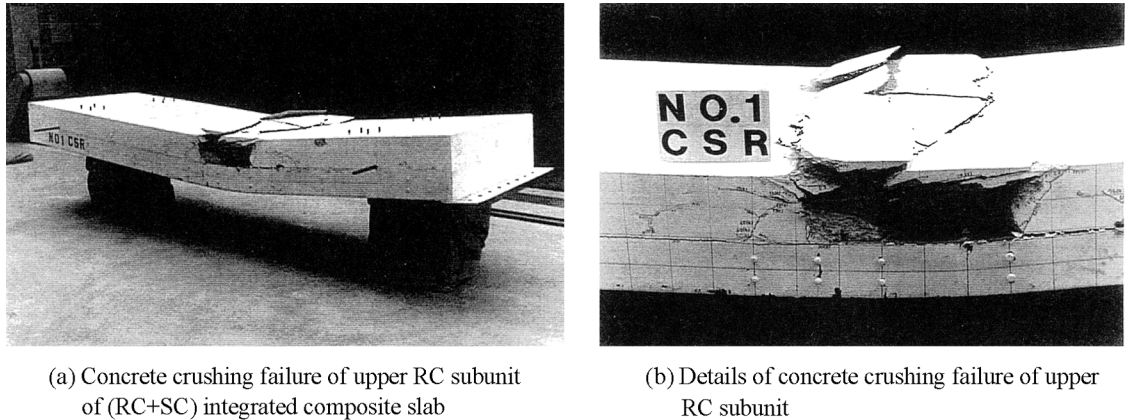


Fig. 14 Flexural strength test specimen No. 1 after failure

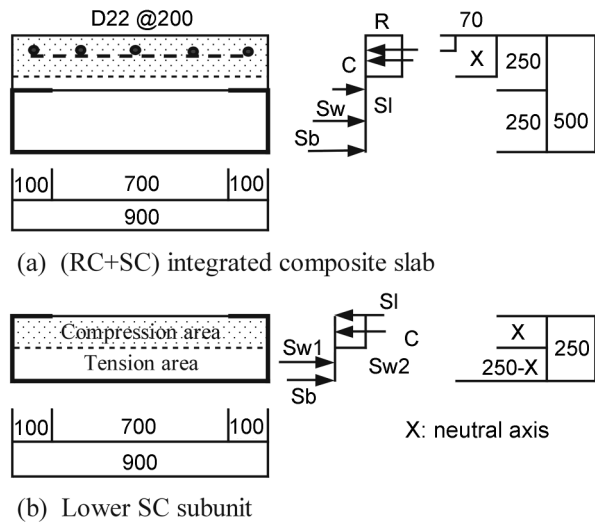


Fig. 15 Computation model for ultimate strength of (RC+SC) integrated composite slab and lower SC subunit

for steel, as shown in Fig. 15 (JSCE, 1989). Fig. 16 depicts idealized bi-linear expressions of load-deflection relationships using the computed ultimate flexural strength of the (RC+SC) integrated composite slab and those of the lower SC subunit.

An analysis of the load-deflection envelope curves shown in Fig. 10 and a comparison with the bi-linear load-deflection relationships shown in Fig. 16 revealed that, although the upper RC subunit of the composite slab crushed due to extremely severe loading, the ductile lower SC subunit of the composite slab did not crush and supported its load. Therefore, the entire composite slab did not collapse. The lower SC subunit in particular has sufficient energy-absorbing capacity in its inelastic deformation. The flexural strength behavior of the (RC+SC) integrated composite slab leads us to conclude that this composite slab has a secondary structural barrier function in the lower SC subunit that prevents overall

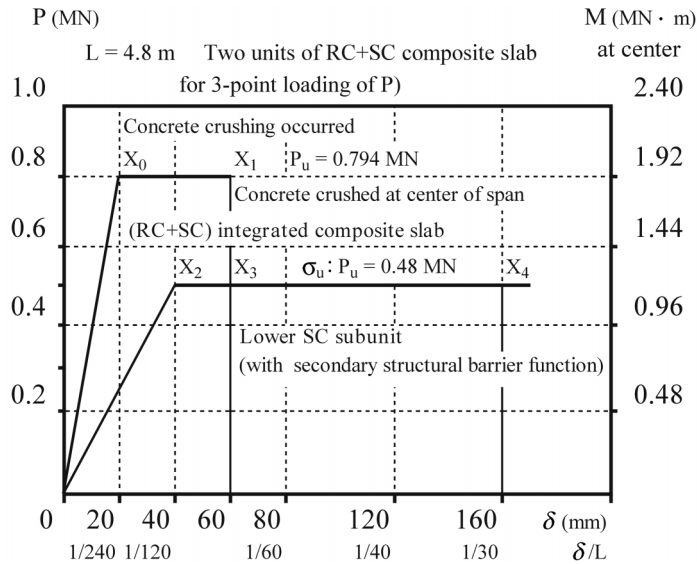


Fig. 16 Bi-linear load-deflection relationships of (RC+SC) integrated composite slab and lower SC subunit

flexural failure.

The flexural strength tests were stopped when it was confirmed that the lower SC subunit in the composite slab maintained its strength beyond the point of  $\delta/L = 1/30$ . Therefore, the (flexural) strength and the deflection at  $\delta/L = 1/30$  of the lower SC subunit were chosen as reference items in considering the concept of the secondary structural barrier function for this (RC+SC) integrated composite slab.

The concept of a structural index was introduced to represent the characteristics of the secondary structural barrier function. From the (flexural) strength and the deflection at  $\delta/L = 1/30$  of the lower SC subunit chosen as reference items, items of the structural index (the (flexural) strength ratio, the ductility factor ratio, and the ratio of the energy-absorbing capacity) of the overall composite slab to the lower SC subunit structure were then chosen as guiding items. These items in the structural index used to evaluate the efficiency of the capacity of the structural barrier function are correlated.

The proposed guiding items in the structural index were investigated to define the secondary structural barrier function of this composite slab structure. These were also examined by the idealized bi-linear load-deflection relationships (lines:  $0-X_0, X_0-X_1$ ) of the (RC+SC) integrated composite slab and those (lines:  $0-X_2, X_2-X_4$ ) of the lower SC subunit shown in Fig. 16. Fig. 17 shows these individual items and their relationships: the (flexural) strengths of  $S_a$  and  $S_b$ , the ductility factors of  $\mu_a$  and  $\mu_b$ , and the energy-absorbing capacities of  $E_a$  and  $E_b$ , for the (RC+SC) integrated composite slab and the lower SC subunit, respectively.  $E_a$  and  $E_b$  correspond to the trapezoidal area of  $(0-X_0-X_1-X_3')$ , and to the rectangular area of  $(X_3'-X_3-X_4-X_4')$ . A common reference deflection of  $\delta_1$  at the (flexural) strength point in the bi-linear load-deflection relationships of the (RC+SC) integrated composite slab was chosen in computing ductility factors  $\mu_a = \delta_2/\delta_1$  and  $\mu_b = \delta_3/\delta_1$ .

These guiding items in the structural index on the concept of the secondary structural barrier function of the (RC+SC) composite slab are defined below.

- 1) Flexural strength ratio:  $S_b/S_a$

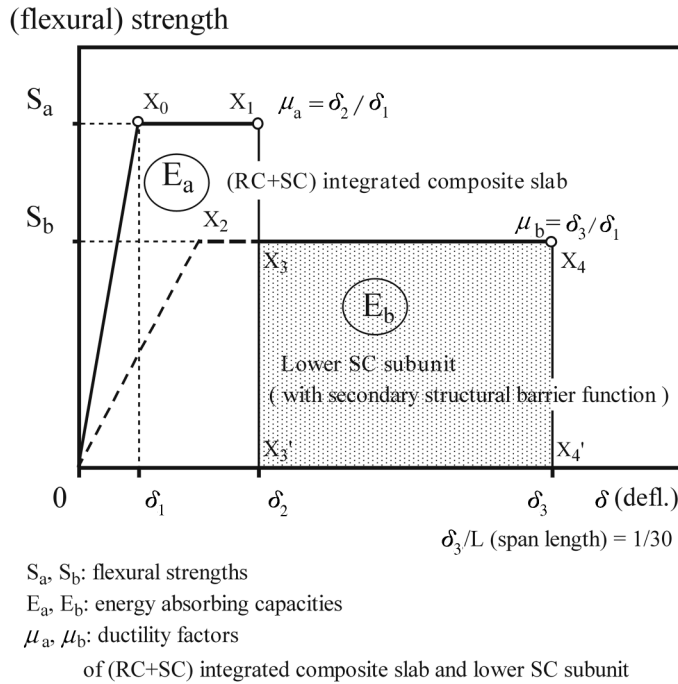


Fig. 17 Items in structural index of (RC+SC) integrated composite slab and lower SC subunit

- a)  $S_b / S_a = 1.0$ : the (RC+SC) integrated composite slab resists a severe load as a one-unit (RC+SC integrated) composite structure, therefore, it has no secondary structural barrier function in the lower SC subunit.
- b)  $0.7 < S_b / S_a < 1.0$ : Almost the same as the above.
- c)  $0.3 < S_b / S_a \leq 0.7$ : The (RC+SC) integrated composite slab has an effective secondary structural barrier function in the lower SC subunit, depending on the amount of its ductility or its energy-absorbing capacity.
- d)  $S_b / S_a \leq 0.3$ : The (RC+SC) integrated composite slab has a relatively poor secondary structural barrier function in the lower SC subunit as its energy-absorbing capacity is small, even though the SC subunit has enough ductility.

2) Ductility factor ratio:  $\mu_b / \mu_a$

A larger  $\mu_b / \mu_a$  indicates the (RC+SC) integrated composite slab has a generally more effective secondary structural barrier function in the lower SC subunit when the (flexural) strength ratio of  $S_b / S_a$  is 0.3 to 0.7.

3) Ratio of the energy-absorbing capacity:  $E_b / E_a$

A smaller energy-absorbing capacity,  $E_b$ , of the lower SC subunit indicates its secondary structural barrier function is less effective. Conversely, a larger  $E_b$  indicates a more effective capacity of its secondary structural barrier function. As a relative evaluation, a larger  $E_b / E_a$  indicates its secondary structural barrier function is more effective when the (flexural) strength ratio of  $S_b / S_a$  is 0.3 to 0.7.

Table 8 presents the computed values for the guiding items of the structural index applied to this composite slab to evaluate the secondary barrier function in the lower SC subunit. The ratios of the (flexural) strength, the ductility factor, and the energy-absorbing capacity of the composite slab to those

Table 8 Computed values for guiding items of structural index for secondary structural barrier function

No.	Guiding item of structural index	Expressions	Computed values
1	(Flexural) Strength ratio	$\frac{S_b}{S_a}$	0.6
2	Ductility ratio	$\frac{\mu_b}{\mu_a}$	2.7
3	Ratio of energy-absorbing capacity	$\frac{E_b}{E_a}$	1.2

$S_a, S_b$ : (flexural) strengths

$E_a, E_b$ : energy absorbing capacities

$\mu_a, \mu_b$ : ductilities of (RC+SC) integrated composite slab and lower SC subunit

of the lower SC subunit were  $S_b/S_a = 0.6$ ,  $\mu_b/\mu_a = 2.7$ , and  $E_b/E_a = 1.2$ . Judging from the general meanings of these items explained above and their values evaluated by the test results, the (RC+SC) integrated composite slab has an effective secondary barrier function in the lower subunit for very severe loading. These values can be the guiding values in determining the efficiency of the secondary structural barrier function in the lower SC subunit for similar types of composite slabs.

More experimental data and analytical parameter studies are required to define the structural index that explains the secondary structural barrier function of the SC subunit structure for this composite slab. The concept of the secondary structural barrier function proposed is applicable to structures for which flexural failure precedes shear failure.

## 6. Example problem

We use the case of an RC shield block falling onto a floor slab after slipping out from the hook of a driving crane during a plant inspection as an example. This type of event is not considered to be a design-based event because of the least-occurrence probability.

The secondary structural barrier function of this composite slab operates for large impact loads that would result from an RC shield block falling on the slab. The equivalent static impact load  $P_{max}$  from falling rocks (stones) is computed from Eq. (2), which is evaluated for dynamic impact loads to static impact loads (using units of meter and tonf) and is referred to in JSCE (1993).

$$P_{max} = 2.455 \cdot W^{2/3} \cdot \lambda^{2/5} \cdot H^{3/5} \quad (2)$$

where  $W$  is the weight of the falling RC block (tf),  $H$  is the height of the fall (m),  $\lambda$  is the constant (tf/m<sup>2</sup>), and values of 700 to 1000 are chosen for the hard surface (RC floor) in the example. The equation is derived from the impact load that results from the collision of the two elastic spherical bodies.

If an RC shield block of 2 tf (0.02 MN) falls from a height of 5 m onto the composite floor slab as shown in Fig. 18, equivalent static impact loads of 141 tf ( $\lambda = 700$ ) to 162 tf ( $\lambda = 1000$ ), (1.38 to 1.59 MN), are computed from Eq. (2). Assuming that this impact load is applied at the center of the composite slab of one unit, the moment at the center span is  $M_c = PL/4$ . However, the experimental data obtained from the three points loading at the span of  $L$  indicated that the central moment is  $M_c = PL/2/2 = PL/4$ . Therefore, the moment at the center span is the same, and thus a similar experimental load-deflection ( $P-\delta$ ) curve can be assumed. The average value of 1.49 MN, computed from 1.41 and 1.62 MN, is

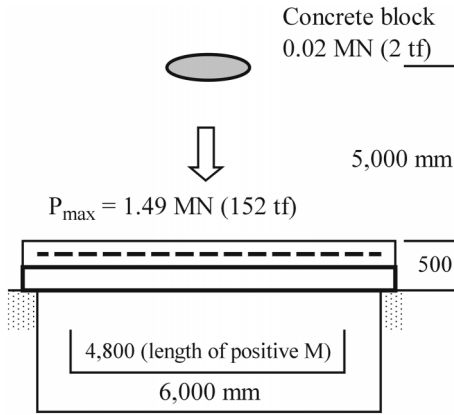


Fig. 18 Example of extremely severe loading

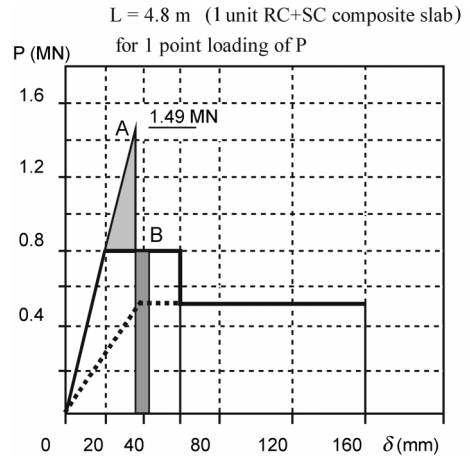


Fig. 19 Strength evaluation of (RC+SC) composite slab subjected to impact load of 149 MN

applied at point A in the idealized  $P-\delta$  curve. Point B is then obtained by an energy equivalent method of the energy-absorbing capacity (as shown in Fig. 19).

The upper RC subunit would be crushed, but the lower SC subunit would still maintain the load-bearing capacity and energy-absorbing capacity, as shown in Fig. 19. Therefore, the composite slab would not lose its load-bearing capacity for extremely severe loading, which indicates that the (RC+SC) integrated composite slab has a secondary structural barrier function in the SC subunit for extremely severe loading.

Finally, by a simple assumption, shear strength  $Q_p$  of the lower SC subunit is computed by Eq. (3) to confirm that its flexural failure precedes shear ultimate (rupture) failure.

$$Q_p = A_c \cdot f_p + A_s \cdot \sigma_u / \sqrt{3} \tag{3}$$

where  $A_c$  and  $A_s$  are the cross sectional areas of the concrete and steel channel.  $f_p$  is the stress at the shear strength of the concrete.  $\sigma_u$  is the tensile strength of the steel (Table 3) and  $\sigma_u / \sqrt{3}$  is the assumed shear rupture strength of the steel.

If we neglect the concrete shear strength for simplicity, we can compute the steel channel shear rupture strength by assuming that the steel channel is cut off in one cross section of the steel channel. Then

$$A_s = 2 \times 25 \text{ (web depth)} \times 06 \text{ (thickness)} + 90 \text{ (width of bottom plate)} \times 0.6 = 72 \text{ cm}^2$$

$$Q_p \doteq A_s \cdot \sigma_u / \sqrt{3} = 72 \text{ cm}^2 \times 426 \text{ MPa} / 1.732 = 1.77 \text{ MN} > 1.49 \text{ MN}$$

We can confirm that flexural failure precedes shear failure for the lower SC subunit structure.

## 7. Conclusions

A new composite slab system of the (RC+SC) integrated composite slab was proposed that uses a large-lipped steel channel with headed studs welded to the bottom plate and reinforced concrete. Full-scale concrete pouring and flexural strength tests were conducted to clarify the structural characteristics

of the proposed composite slab.

The proposed composite slab can be used as an unsupported form to accept poured concrete loads. The initial stress on the steel plate caused by the concrete load in the tests had no influence on the strength or deflections of the composite slab before it reached its ultimate strength. The load-deflection relationship at the center of the composite slab can be evaluated on the basis of the conventional beam theory. Flexural strength tests confirmed that this new composite slab system has excellent strength and ductility characteristics, making it ideal as a structural barrier as well as a primary load-bearing unit, providing construction cost savings for contractors.

The concept of a secondary structural barrier function of the lower SC subunit of this composite slab structure was also proposed in this study and explained by a simple sample problem. However, further study is required regarding the mechanism of the structural barrier function of the lower SC subunit of the composite slab structure, and also to resolve the structural index that represents the characteristics of the structural barrier function.

## Acknowledgements

A part of the work was carried out in Kajima Corporation. Prof. Kato B., Dr. Sato K., Dr. Toyama K., Mr. Kobayashi M., Mr. Ishii K., and Dr. Fukumoto T., are deeply acknowledged.

## References

- AISC (1999), *Load and Resistance Factor Design Manual of Steel Construction*, Chicago.
- Architectural Institute of Japan (AIJ) Standard (1998), *Design standard for Steel Structures*, Tokyo.
- ASCE (1991), *Standard for the Structural Design of Composite Slabs/ Standard Practice for Construction and Inspection of Composite Slabs*, ANSI/ASCE 9-91, New York.
- Buckner, C.D. (Subcommittee chairman), Alsamsam, E., Clawson, W.C., Darwin, D., Donahey, R.C. and Easterling, W.S. (2002), "Construction considerations for composite steel-and-concrete floor systems", Subcommittee on composite steel and concrete Floor Systems of the Committee on Composite Construction of the Technical Administrative Committee on Metals, *J. Struct. Eng.*, ASCE, September, 1099-1110.
- Emori, K. (1999), "Study of the structural characteristics of a large steel channel and reinforced concrete composite slab system", *Proc. of the 1st International Summer Symposium*, JSCE, Tokyo, Japan, 73-76.
- Emori, K. (2001), "A large steel channel and reinforced concrete composite slab with a secondary structural barrier function", *Proc. of the 1st Int. Conf. on Steel & Composite Structures*, Pusan, Korea, 1213-1220.
- Eurocode 4 (1994), *Design of Composite Steel and Concrete Structures*, CEN.
- Frangopol, D.M. and Curley, J.P. (1987), "Effects of damage and redundancy on structural reliability", *J. Struct. Eng.*, ASCE, July.
- Iyama, J. and Kuwamura, H. (1998), "Fail-safe structures to resist earthquakes", *J. Struct. Constr. Engr.*, **507**, AIJ, 29-34.
- Japan Society of Civil Engineers (JSCE) (1989), *Design Guideline for Steel-Concrete Composite Structures, Structural Engineering Series 3*, Tokyo, 153-167.
- JSCE (1993), *Impact Behavior and Design of Structures, Structural Engineering Series 6*, Tokyo, 183-196.
- Kato B., Sato K., Toyama K., Kobayashi M., Ishii K., Fukumoto T and Emori K. (1988), "Study on new floor slab composed of concrete and lipped large channel steel", *Summaries of Technical Papers of Annual Meeting (Kanto)*, AIJ, Japan.
- Ma, K.J., Xiao, J.C., Zhang, H.A., Zhang, H.P., Zhang, Ha., Qi, X. and Bai, F.J. (2001), "A new type of steel-concrete composite plate", *Proc. of 6th Pacific Structural Steel Conference*, Beijing, China, **2**, 1070-1075.

- McDonald, D.G., Watson, K.B. and Hunt, D.S. (1995), "Unifloor - a new steel and concrete domestic flooring system", *Proc. of 4th Pacific Structural Steel Conference*, Singapore, **3**, 137-144.
- Muto, K. (1964), *Plastic Design for Reinforced Concrete Structures, Earthquake Resistant Design Series 2*, Maruzen Co., Tokyo, Japan, 41.
- Patrick, M., Goh, C.C. and Proe, D.J. (1995), "Limit-state design rules for Bondeck II composite slabs", *Proc. of 4th Pacific Structural Steel Conference*, Singapore, **3**, 145-152.

CC